RESEARCH ARTICLE

Figures and figure supplements

Organelle proteomic profiling reveals lysosomal heterogeneity in association with longevity

Yong Yu *et al*.

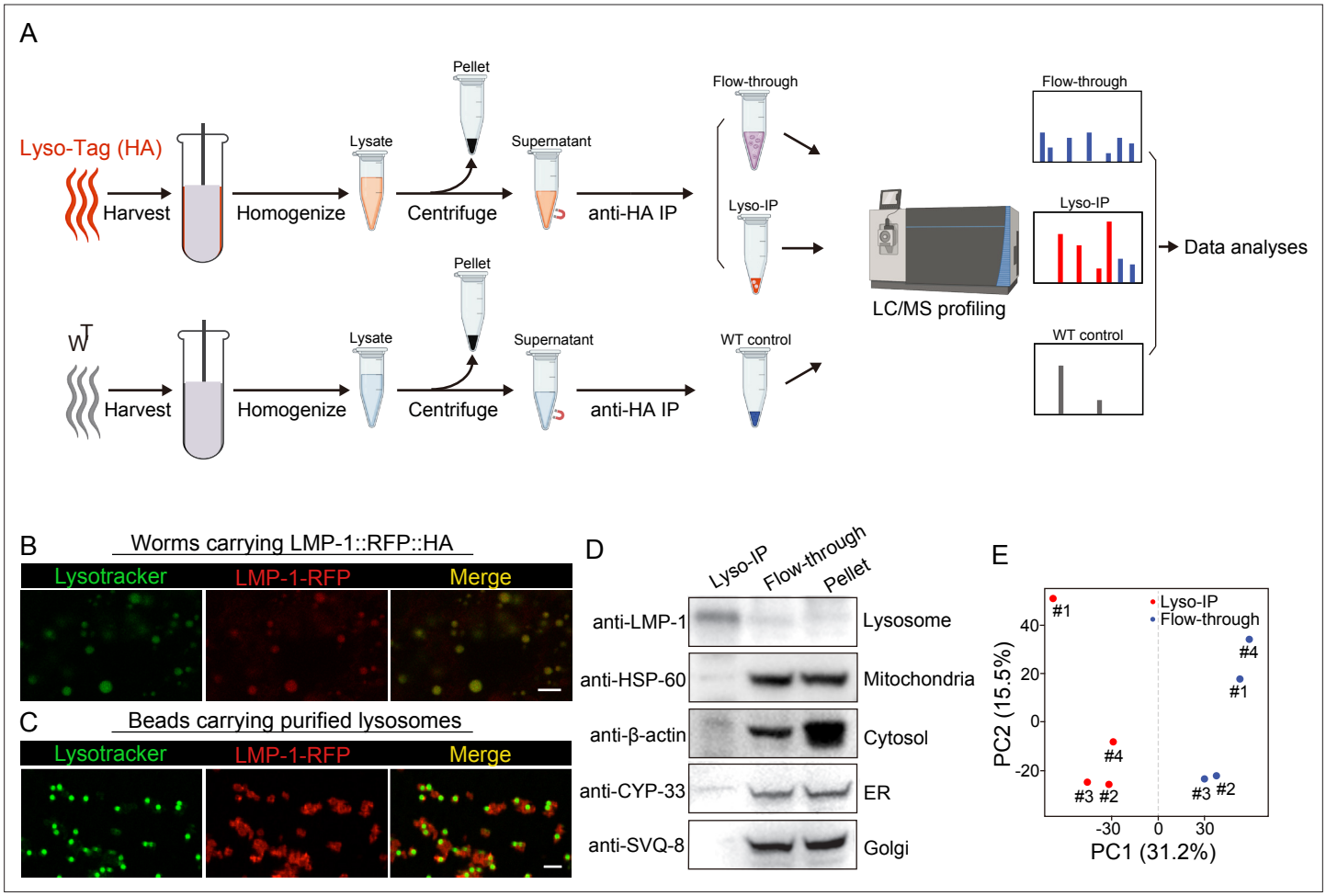

Figure 1. Rapid lysosome isolation coupled with proteomic profiling. (**A**) Schematic of the workflow for immunoprecipitation-based lysosome purification (Lyso-IP) and mass-spectrometry based proteomic profiling to identify lysosome-enriched proteomes in *C. elegans*.(**B**) Example images of transgenic strains carrying LMP-1 Lyso-Tag (LMP-1::RFP-3×HA) with LysoTracker staining to mark lysosomes in vivo. Scale bar = 5 μm. (**C**) Example images of beads carrying purified lysosomes from Lyso-IP with LysoTracker staining to mark intact lysosomes in vitro. Scale bar = 5 μm.(**D**) Western blot for protein markers of different subcellular compartments using purified lysosomes (Lyso-IP), paired non-lysosomal fractions (Flow-through) or Pellet. (**E**) PCA analysis of four independent biological replicates of Lyso-IP and Flow-through samples.

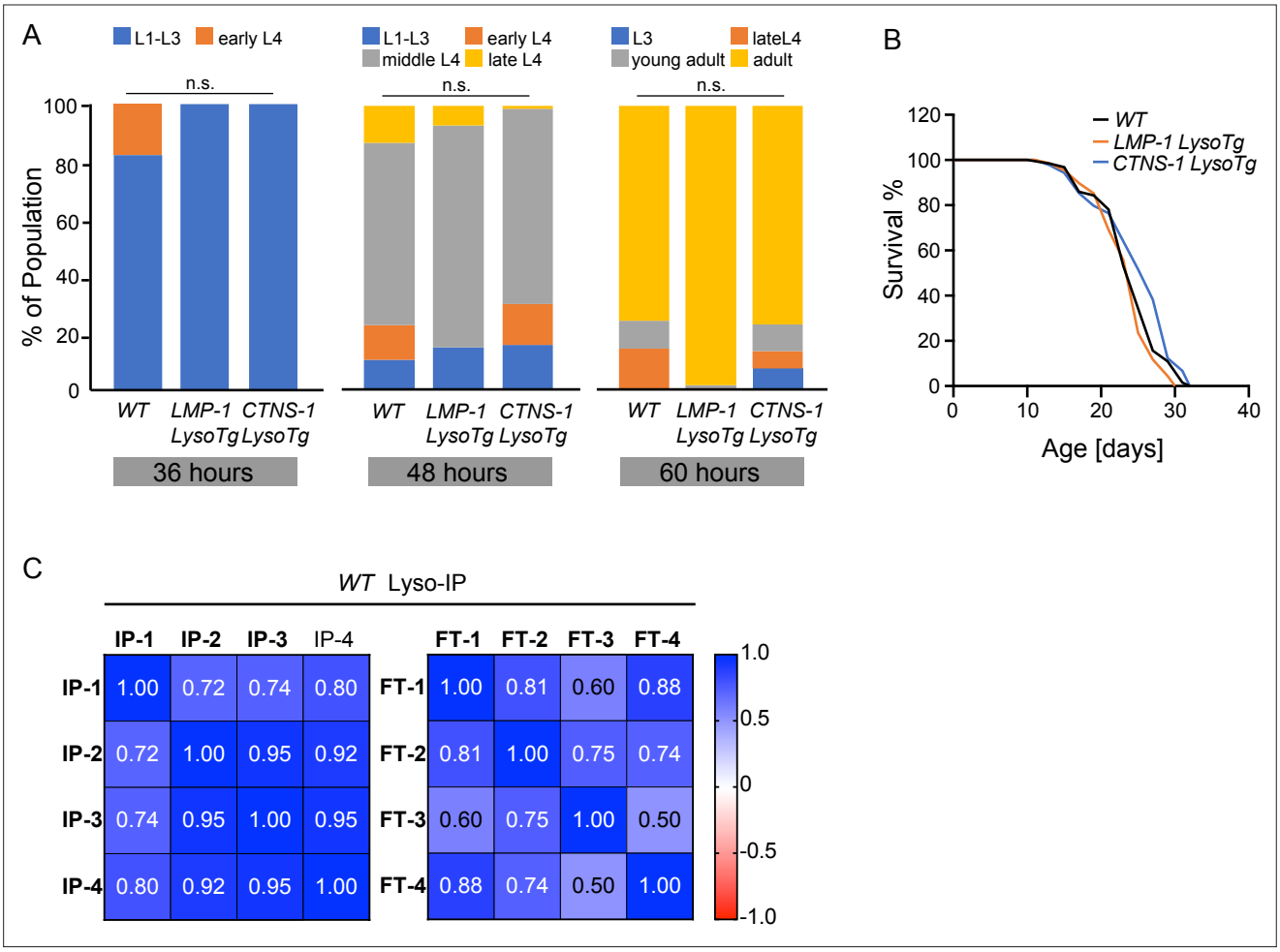

Figure 1—figure supplement 1. Analysis of *LysoTg* lines and Lyso-IP profiling in wild-type worms. (**A**) Developmental timing of WT and transgenic strains expressing LMP-1 and CTNS-1 Lyso-Tag (LMP-1 and CTNS-1 *LysoTg*). n.s. *P>0.05* by Chi-squared test. (**B**) Lifespan of WT, LMP-1 *LysoTg*, and CTNS-1 *LysoTg* worms. The lifespan data are also in ***Supplementary file 8***. (**C**) Correlation analysis of four independent biological replicates of Lyso-IP (IP) and Flow-through (FT) samples from proteomics analyses.(***Nakae et al., 2010***)

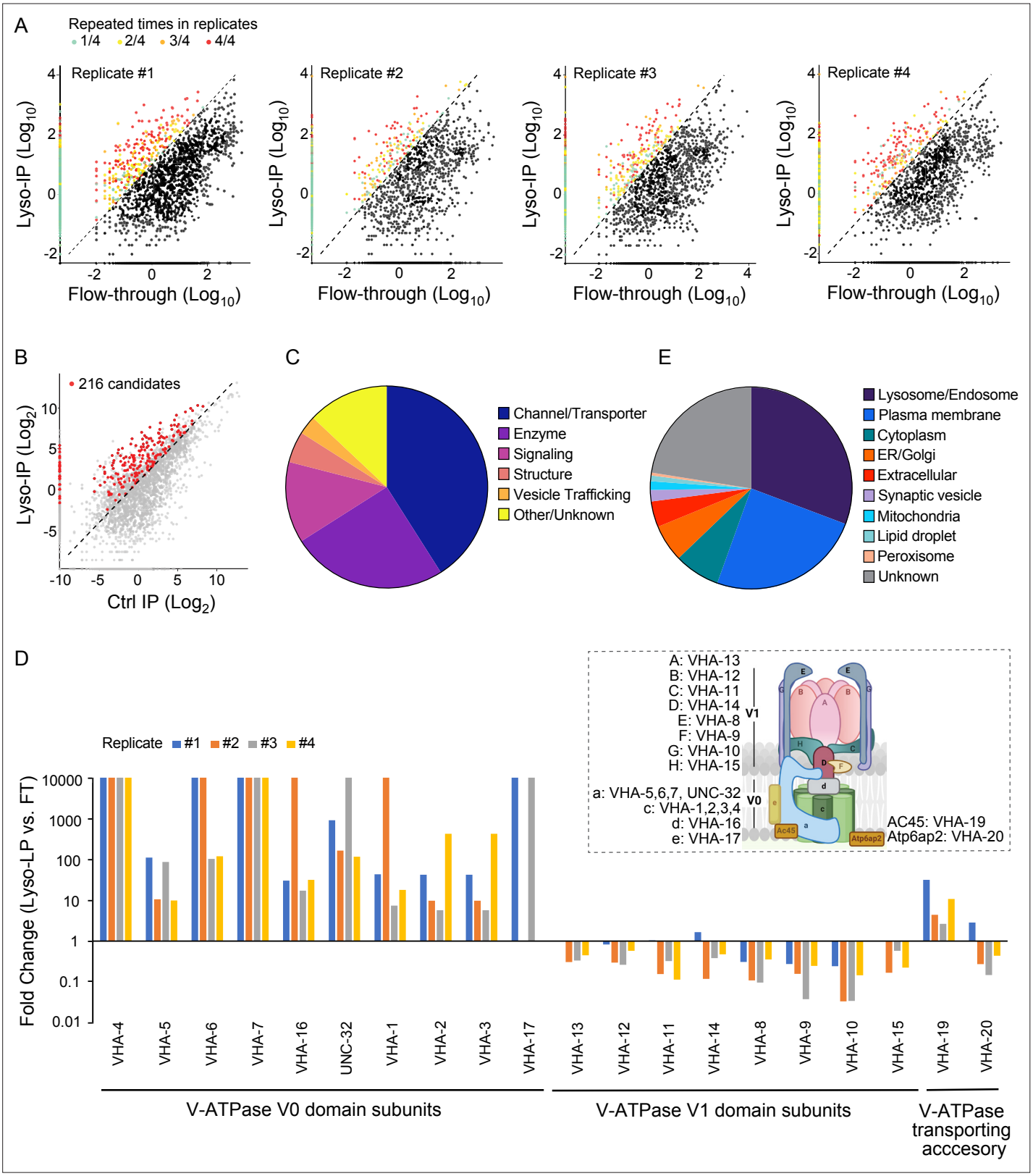

Figure 2. Systematic view of lysosome-enriched proteome. (**A**) Scatter plots showing candidate selection from four independent biological replicates in proteomics analyses. Proteins with at least 10-fold higher levels in Lyso-IP samples than in flow-through (FT) controls are highlighted with different colors based on repeated times in four replicates. (**B**) Scatter plot showing candidate selection with normalization to non-tagged controls using wild-type worms. 216 proteins with over 2-fold higher levels in Lyso-IP samples than in non-tagged controls are highlighted in red. (**C**) Pie chart showing molecular

Figure 2 continued on next page

Figure 2 continued

function categories of lysosome-enriched proteins. (**D**) The lysosomal enrichment ratio (Lyso-IP vs FT) for each subunit of lysosomal vacuolar ATPase (v-ATPase) in four independent replicates is shown. Inserted scheme showing lysosomal V-ATPase assembly.(**E**) Pie chart showing subcellular location categories of lysosome-enriched proteins.

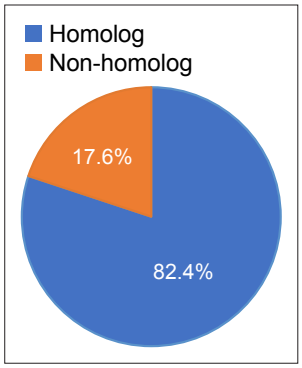

Figure 2—figure supplement 1. Pie chart showing the proportion of LMP-1 Lyso-IP candidates from WT worms with mammalian homologs.

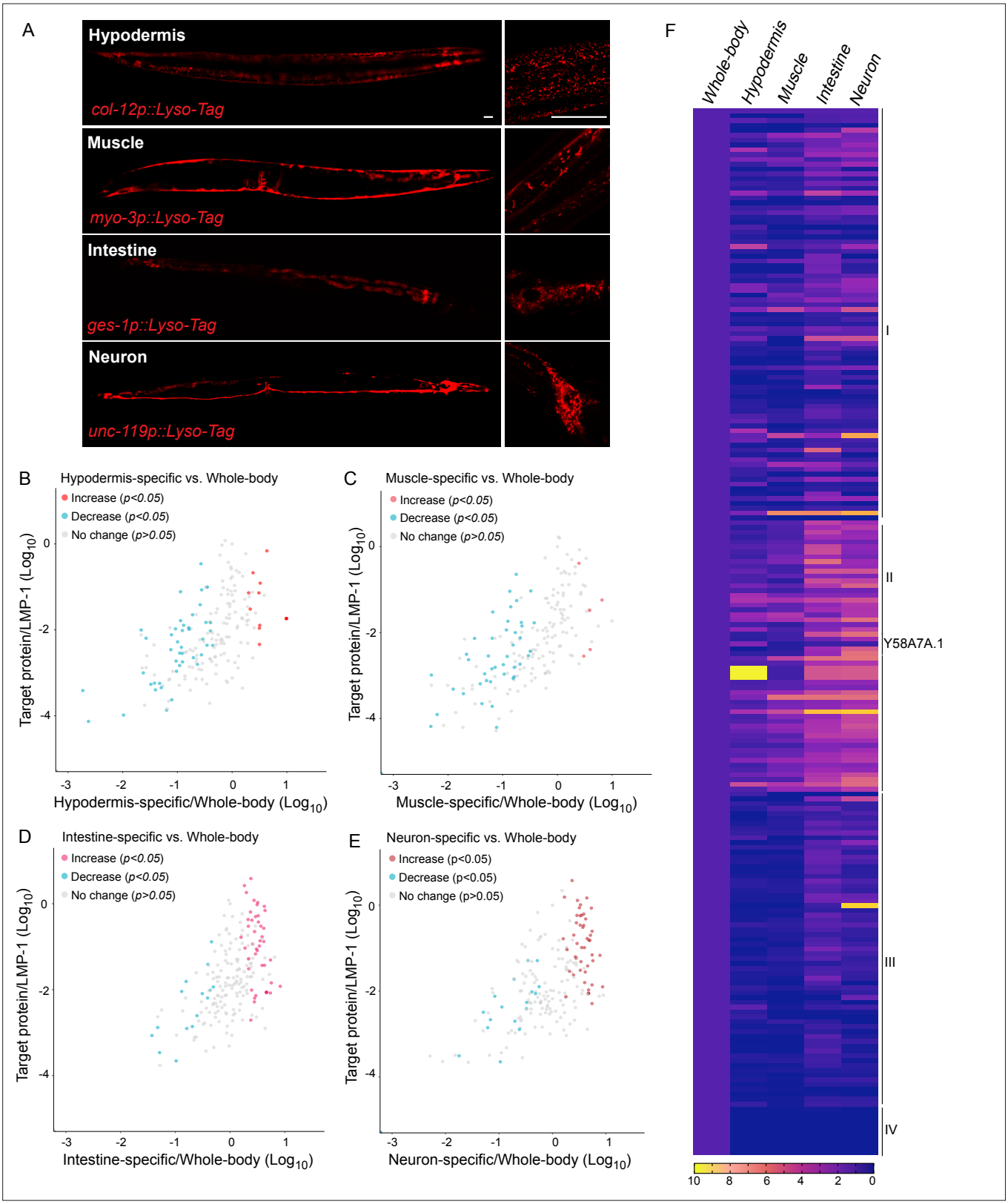

Figure 3. Lysosomal proteome heterogeneity across tissues. (**A**) Example images of transgenic strains carrying Lyso-Tag (LMP-1::RFP-3×HA) driven by four different tissue-specific promoters. Scale bar =20 μm. (**B–E**) Scatter plot showing the relative enrichment ratio for each of 216 lysosome-enriched proteins identified from whole-body LMP-1 Lyso-IP in comparison with tissue-specific LMP-1 Lyso-IPs, hypodermis (**B**), muscle (**C**), intestine (**D**) and neuron (**E**). X axis, enrichment ratio tissue-specific vs. whole-body; Y axis, normalized protein abundance over LMP-1; each dot represents the average

Figure 3 continued on next page

Figure 3 continued

of three replicates. (**F**) Heatmap showing the relative enrichment of 216 lysosome-enriched proteins identified from whole-body LMP-1 Lyso-IP in comparison with tissue-specific LMP-1 Lyso-IPs. Group I, comparable ratios between whole-body and tissue-specific Lyso-IPs; Group II, increase in tissue-specific Lyso-IPs ($P<0.05$ by student's t-test); Group III, decrease in tissue-specific Lyso-IPs ($P<0.05$ by student's t-test); Group IV, absent in tissue-specific IPs.

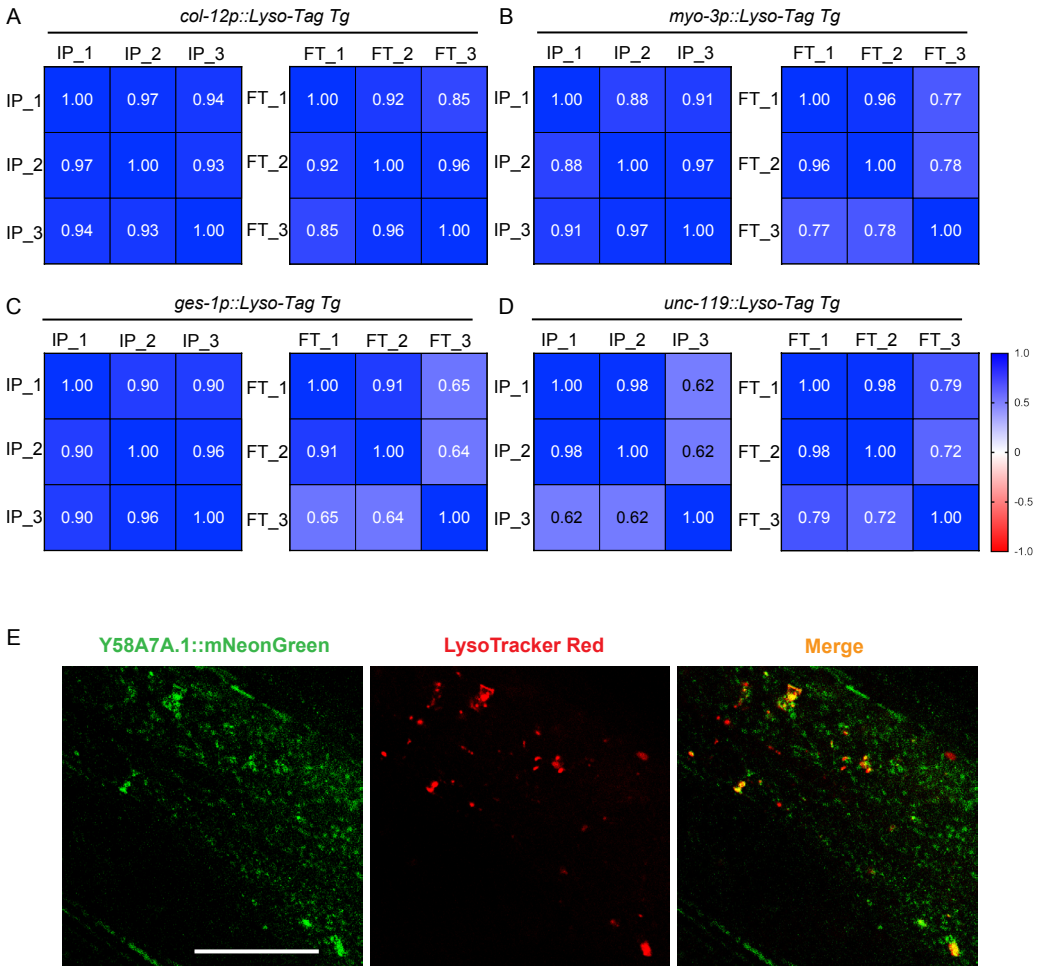

Figure 3—figure supplement 1. Tissue-specific Lyso-IPs and candidate imaging. (**A–D**) Pearson Correlation matrices of tissue-specific lyso-IP (IP) samples and flow-through (FT) samples show the correlation among three different replicates. (**A**) Hypodermis, (**B**) Muscle, (**C**) Intestine, (**D**) Neuron. (**E**) Representative images showing colocalization of Y58A7A.1::mNeonGreen and LysoTracker Red in the hypodermis. Scale bar = 20 μm.

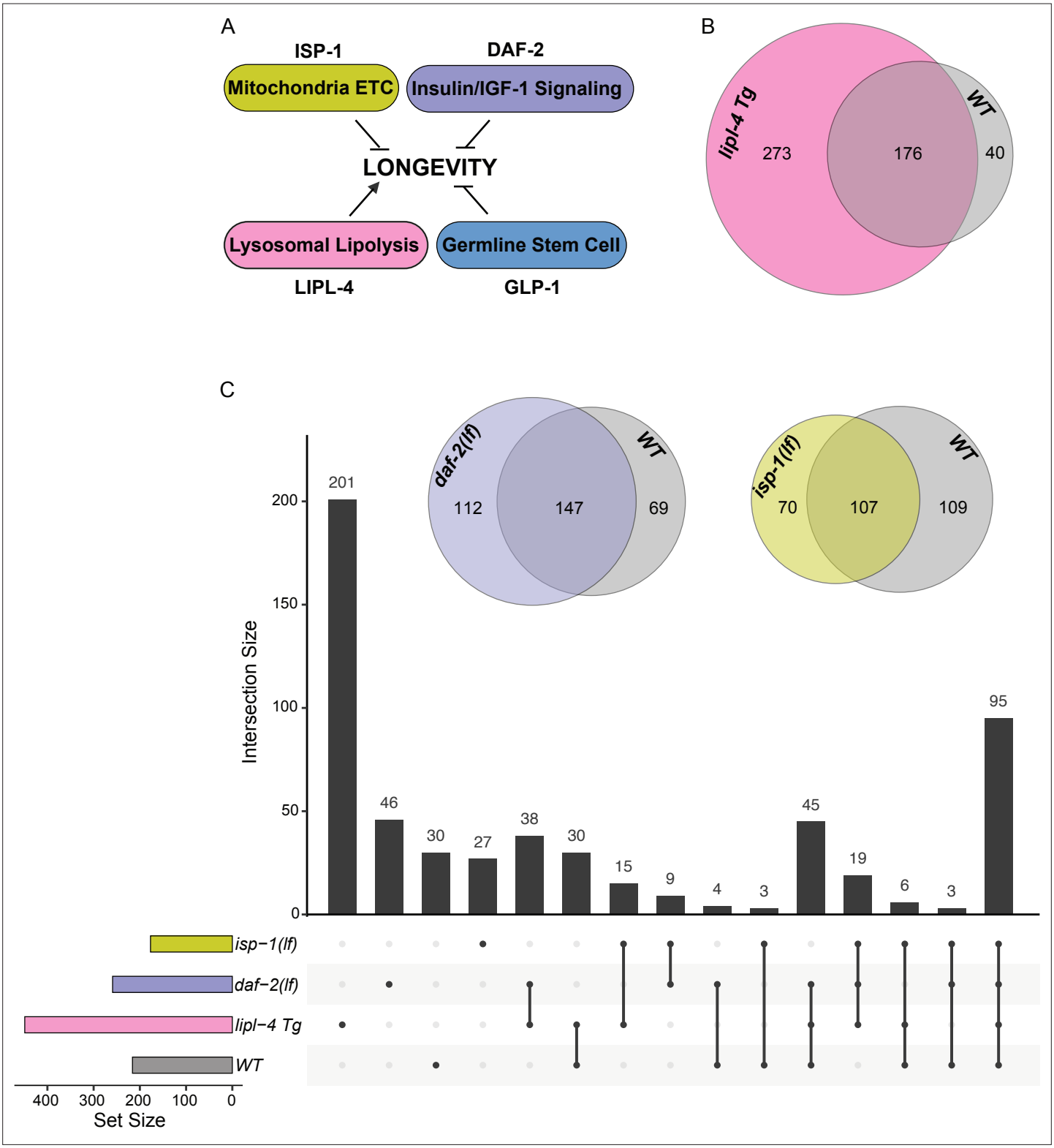

Figure 4. Lysosomal proteome in different pro-longevity models. (**A**) Scheme showing four different longevity regulatory mechanisms used in this study. Loss-of-function mutants (lf) of *isp-1, daf-2,* and *glp-1* reduce mitochondrial electron transport chain (ETC) complex III, insulin/IGF-1 signaling, and germline stem cell proliferation, respectively, leading to lifespan extension; while increasing lysosomal lipolysis by *lipl-4* transgenic overexpression (*lipl-4 Tg*) promotes longevity.(**B**) Venn diagram showing the overlap between the lysosome-enriched proteomes from wild-type (WT) and *lipl-4 Tg* worms. (**C**) Upset graph showing the distribution and overlap of lysosome-enriched proteins across the four pro-longevity models. Inserted Venn diagram showing the overlaps between the lysosome-enriched proteomes of WT worms and the long-lived *daf-2(lf)* and *isp-1(lf)* mutants.

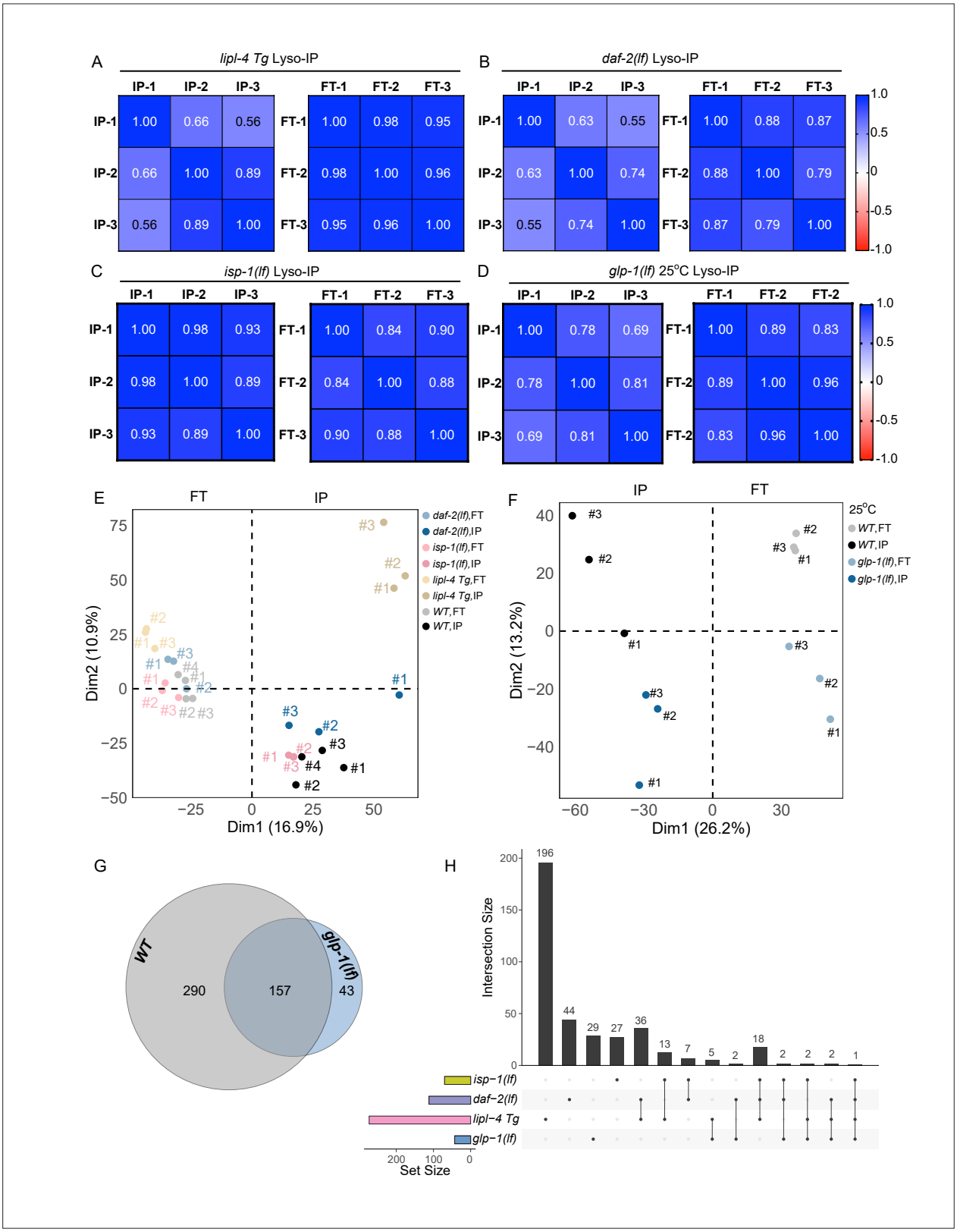

Figure 4—figure supplement 1. Lyso-IP analyses from different long-lived strains. (**A–D**) Correlation analysis of three independent biological replicates of Lyso-IP (IP) and Flow-through (FT) from proteomics analyses of the long-lived *lipl-4* transgenic strain *lipl-4 Tg*, (**A**), the *daf-2* loss-of-function mutant (*daf-2(lf)*), (**B**), the *isp-1* loss-of-function mutant (*isp-1(lf)*), (**C**) and *glp-1* loss-of-function mutant grown in 25°C (*glp-1(lf)*) 25°C, (**D**). (**E**) PCA analysis of Lyso-IP replicates (IP) and flow-through controls (FT) in LMP-1 Lyso-IP of WT, *lipl-4 Tg*, *daf-2(lf)*, and *isp-1(lf)* worms. (**F**) PCA analysis of Lyso-IP replicates (IP)

Figure 4—figure supplement 1 continued on next page

Figure 4—figure supplement 1 continued

and flow-through controls (FT) in LMP-1 Lyso-IP of WT and *glp-1(lf)* worms grown at 25°C. (**G**) Venn diagram showing the overlap between the lysosome-enriched proteomes from WT and *glp-1(lf)* worms grown at 25°C. (**H**) Upset graph showing the overlap of lysosome-enriched proteins present in the long-lived worms but absent from WT worms.

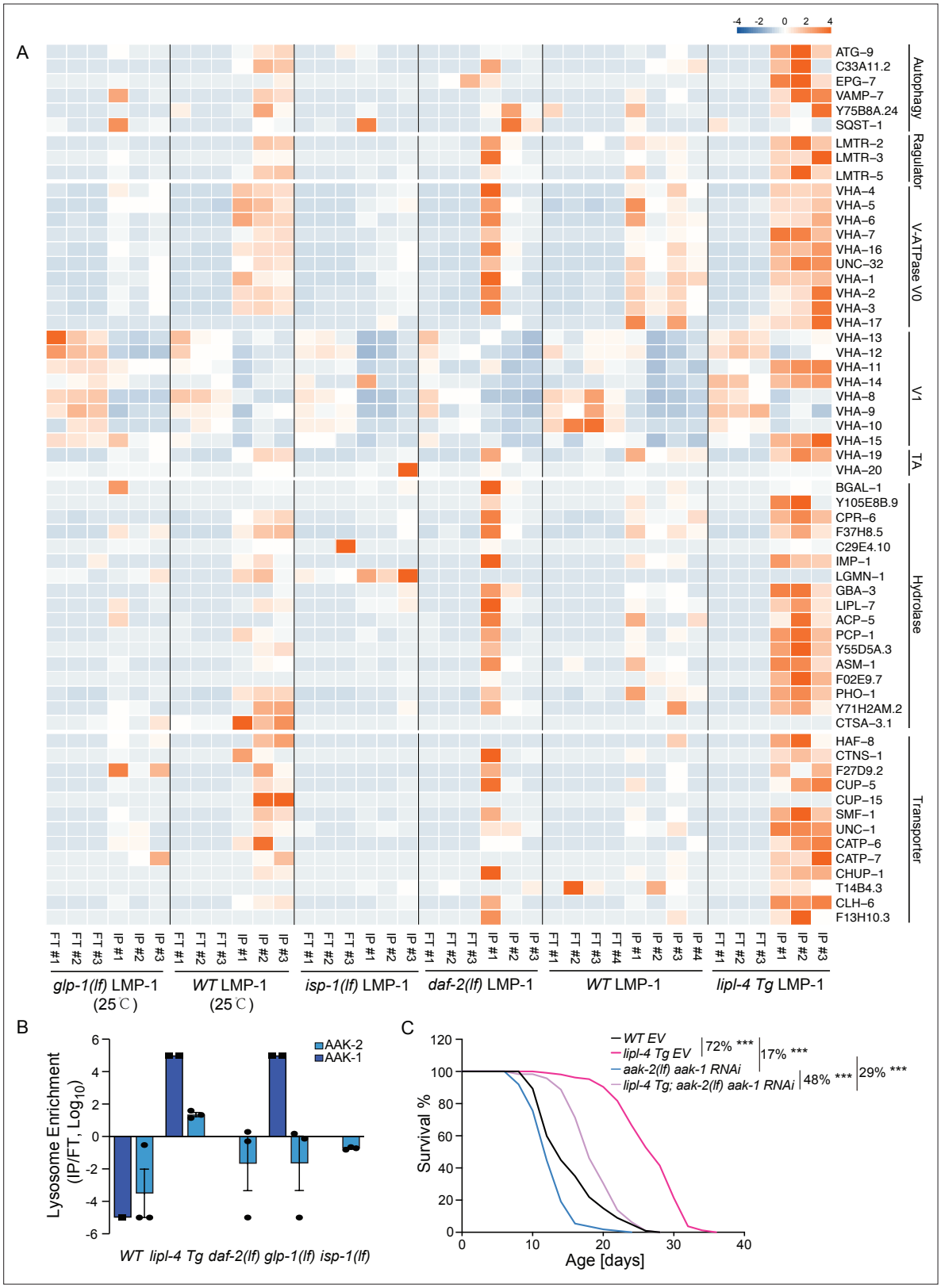

Figure 5. Increased enrichment of lysosomal proteins upon lysosomal lipolysis. (**A**) Normalized protein levels (z-score across samples) of autophagy-related components, mTORC1 signaling factors, lysosomal v-ATPase V0, V1, and transporting accessory (TA) subunits, lysosomal hydrolases and transporter proteins from LMP-1 Lyso-IP proteomic analyses of WT, *lipl-4 Tg, daf-2(lf)*), *isp-1(lf)* worms grown at 20°C and WT and *glp-1(lf)* worms grown at 25°C. (**B**) The lysosomal enrichment ratio (Lyso-IP vs FT) for two homologs of AMPK catalytic subunits, AAK-1 and AAK-2 in WT, *lipl-4 Tg, daf-2(lf),*

Figure 5 continued on next page

Figure 5 continued

isp-1(lf) and glp-1(lf) worms. (**C**) Reduction of AMPK using the loss-of-function mutant of *aak-2, aak-2(lf)* together with *aak-1* RNAi knockdown decreases lifespan by 17% and 29% in the WT and *lipl-4 Tg* background, respectively. As a result, the lifespan extension caused by *lipl-4 Tg* is reduced from 72% to 48%. *** *P<0.001* by Log-rank test. The lifespan data are also in ***Supplementary file 8***.

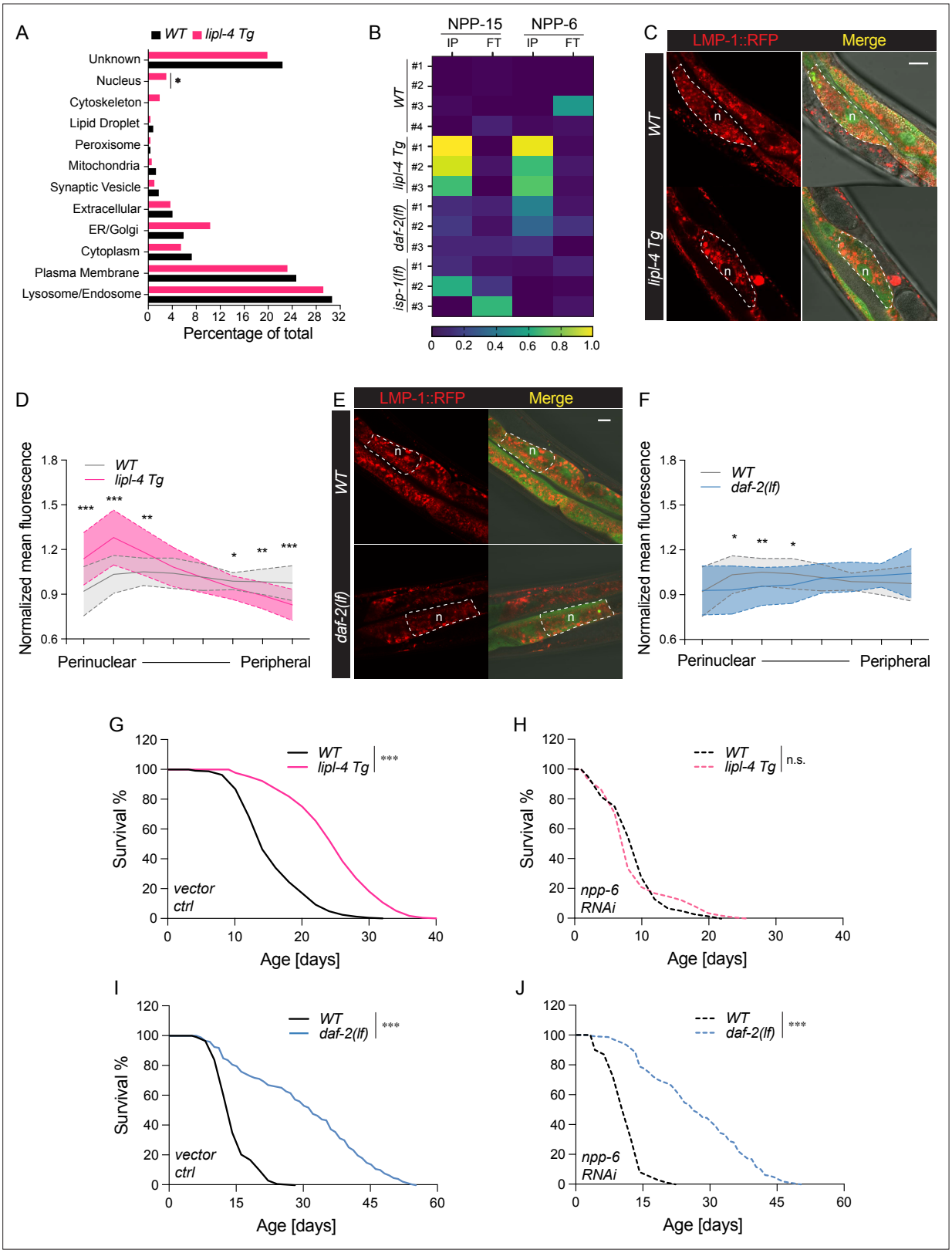

Figure 6. Enhanced lysosome-nucleus proximity contributing to longevity. (**A**) The percentage of proteins with different subcellular localization is compared between lysosome-enriched proteomes from WT and *lipl-4 Tg* worms.* *P*=0.019 by 2-sample test for equality of proportions.(**B**) Heatmap showing the average levels of nucleoporin proteins NPP-6 and NPP-15 in Lyso-IP (IP) and flow-through (FT) samples from WT, *lipl-4 Tg, daf-2(lf),* and *isp-1(lf)* worms. (**C, E**) Representative images of intestinal cells in WT, *lipl-4 Tg* (**C**), and *daf-2(lf)* (**E**) worms carrying LMP-1::RFP-3×HA and nucleus-enriched

Figure 6 continued on next page

Figure 6 continued

GFP, showing the accumulation of lysosomes around the perinuclear region in the *lipl-4 Tg* but not *daf-2(lf)* worms. Dashed lines circle intestinal cells and n marks the nucleus. Scale bar = 20 μm. (**D, F**) Line graph showing the spatial distribution of lysosomes from the nuclear to peripheral region quantified by normalized regional RFP fluorescence signals in intestinal cells of WT, *lipl-4 Tg* (**D**), and *daf-2(lf)* (**F**) worms. N=50 WT /33 *lipl-4 Tg*, 33 WT/28 *daf-2(lf)*. Data are represented as mean ± SD. *p* values for (**D**) (from left to right): $1.23x10^{-7}$, $2.25x10^{-5}$, 0.00322, 0.368, 0.273, 0.0447, 0.00268, $1.20x10^{-5}$; *p* values for (**F**) (from left to right): 0.633, 0.0211, 0.00259, 0.0359, 0.767, 0.151, 0.106, 0.0671.(**G–H**) *lipl-4 Tg* worms show lifespan extension compared to WT worms (**G**), which is fully suppressed by RNAi knockdown of *npp-6* (**H**). ****P<0.001*, n.s. *P>0.05* by Log-rank test. (**I–J**) *daf-2(lf)* worms show lifespan extension compared to WT worms (**I**), which is not affected by *npp-6* RNAi knockdown (**J**). ****P<0.001* by Log-rank test. The lifespan data are also in ***Supplementary file 8***.

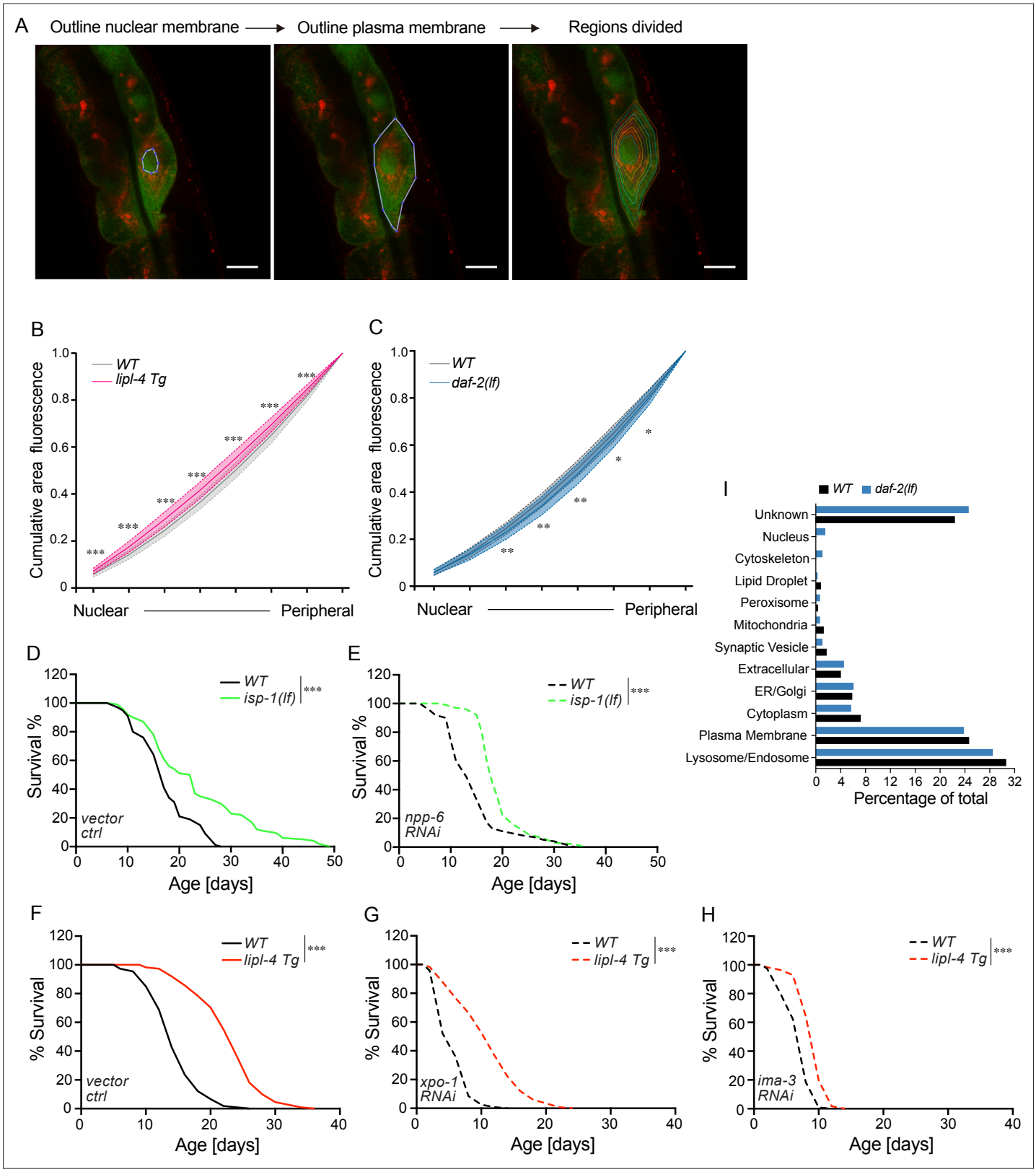

Figure 6—figure supplement 1. Lysosomal positioning in longevity regulation. (**A**) Summary of the method flow for quantifying the lysosomal distribution in intestinal cells of *C.elegans*. Scale bar = 10 μm. (**B, C**) Curve graph showing the normalized accumulated intensity of lysosomal signals from the nuclear to the peripheral region in WT, *lipl-4 Tg* (**B**), and *daf-2(lf)* (**C**) animals. *$P<0.05$; **$P<0.01$, ***$P<0.001$, ****$P<0.0001$, n.s. $P>0.05$ by Student's t-test (unpaired, two-tailed) for each region. N=50 WT /33 *lipl-4 Tg*, 33 WT/ 28 *daf-2(lf)*. Data are represented as mean ± SD. *p* values for

Figure 6—figure supplement 1 continued on next page

Figure 6—figure supplement 1 continued

(**B**) (from left to right): $2.65x10^{-8}$, $3.19x10^{-8}$, $7.93x10^{-8}$, $3.62x10^{-7}$, $4.79x10^{-6}$, $2.98x10^{-5}$, $4.41x10^{-5}$; *p* values for (**C**) (from left to right): 0.357, 0.0529, 0.00611, 0.00246, 0.00985, 0.0261, 0.0423. (**D–E**) *isp-1(lf)* worms show lifespan extension compared to WT worms (**D**), which is not affected by RNAi knockdown of *npp-6* (**E**). ****P<0.001* by Log-rank test. (**F–H**) *lipl-4 Tg* worms show lifespan extension compared to WT worms (**F**), which is not affected by *xpo-1* RNAi knockdown (**G**) and is partially suppressed by RNAi knockdown of *ima-3* (**H**). ****P<0.001* by Log-rank test.The lifespan data are also in ***Supplementary file 8***. (**I**). The percentage of proteins with different subcellular localization is compared between lysosome-enriched proteomes from WT and *daf-2* worms.

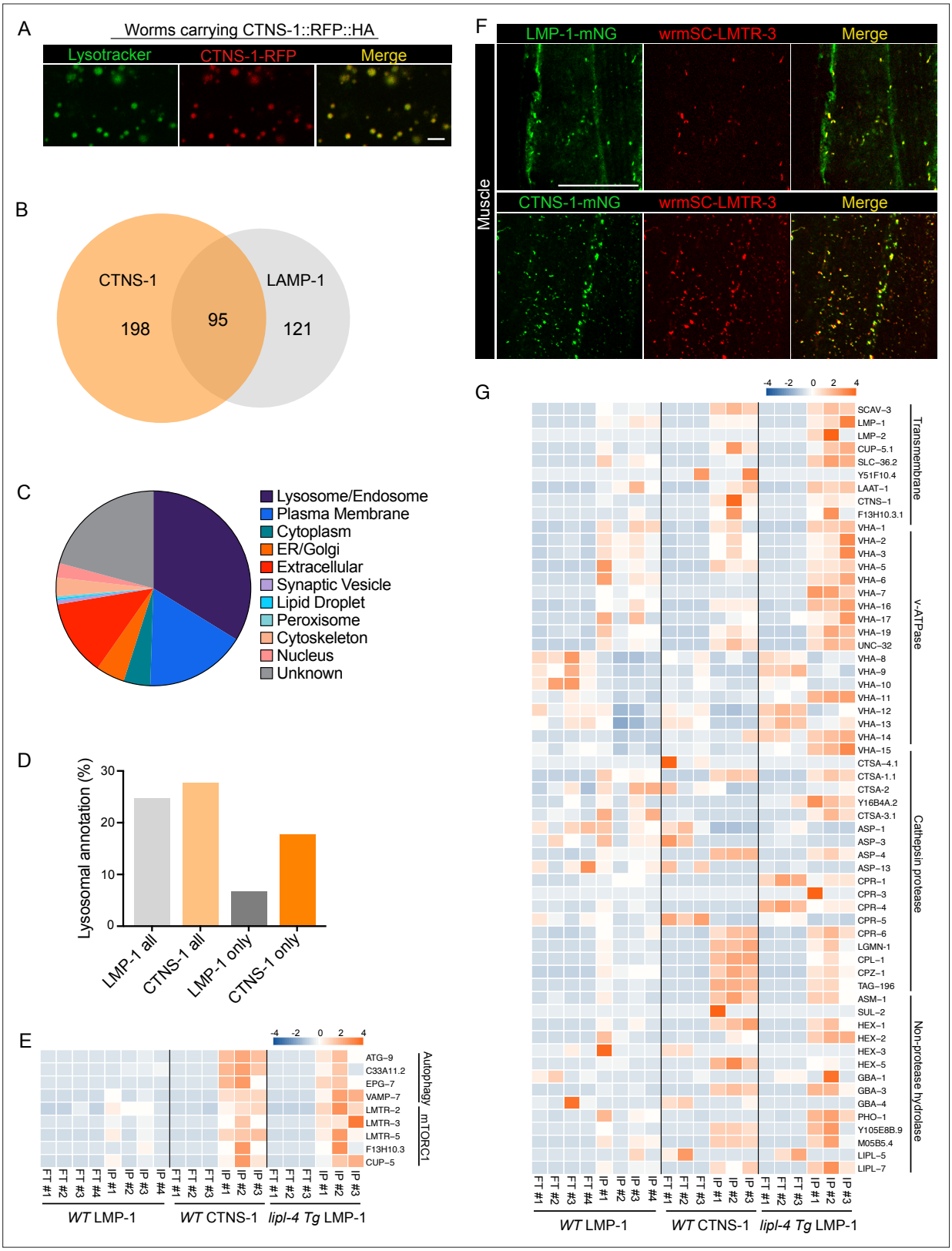

Figure 7. Lysosome-enriched proteome identified with Cystinosin. (**A**) Example images of transgenic strains carrying CTNS-1 Lyso-Tag (CTNS-1::RFP-3×HA) with LysoTracker staining to mark lysosomes in vivo. Scale bar = 5 μm. (**B**) Venn diagram showing the overlap between lysosome-enriched proteomes using LMP-1 Lyso-IP and CTNS-1 Lyso-IP. (**C**) Pie chart showing subcellular location categories of lysosome-enriched proteins.(**D**) The proportion of candidates with lysosomal localization annotation in different candidate groups. 'LMP-1 all' and 'CTNS-1 all', all candidates from LMP-1

Figure 7 continued on next page

Figure 7 continued

Lyso-IP and CTNS-1 Lyso-IP, respectively; 'LMP-1 only' and 'CTNS-1 only', candidates only identified from LMP-1 Lyso-IP or CTNS-1 Lyso-IP, respectively. (**E**) Normalized protein levels (z-score across samples) of autophagy-related components and mTORC1 signaling factors from CTNS-1 Lyso-IP proteomic analyses of WT worms and LMP-1 Lyso-IP proteomic analyses of WT and *lipl-4 Tg* worms. (**F**) Representative muscle images in the wrmScarlet::LMTR-3 knock-in line crossed with either LMP-1::mNeonGreen knock-in line or CTNS-1::mNeonGreen knock-in line. Scale bar = 20 μm.(**G**) Normalized protein levels (z-score across samples) of previously annotated lysosomal proteins from LMP-1 Lyso-IP proteomic analyses of WT and *lipl-4 Tg* worms and CTNS-1 Lyso-IP proteomic analyses of WT worms.

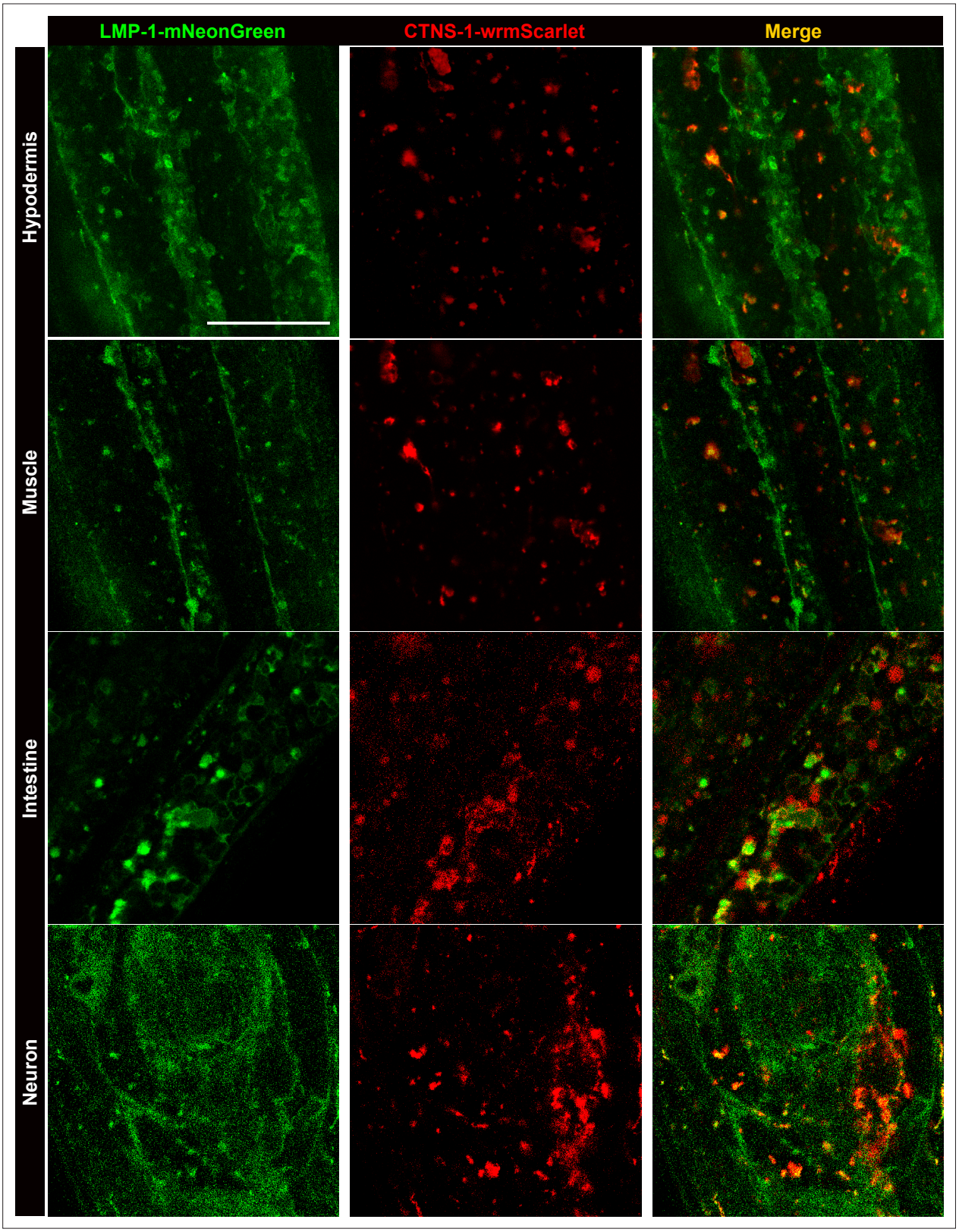

Figure 7—figure supplement 1. The colocalization between LMP-1::mNeonGreen and CTNS-1::wrmScarlet in different tissues. Representative images of knock-in lines with both LMP-1::mNeonGreen and CTNS-1::wrmScarlet show partial colocalization between LMP-1 and CTNS-1 signals in different tissues. Scale bar = 20 μm.

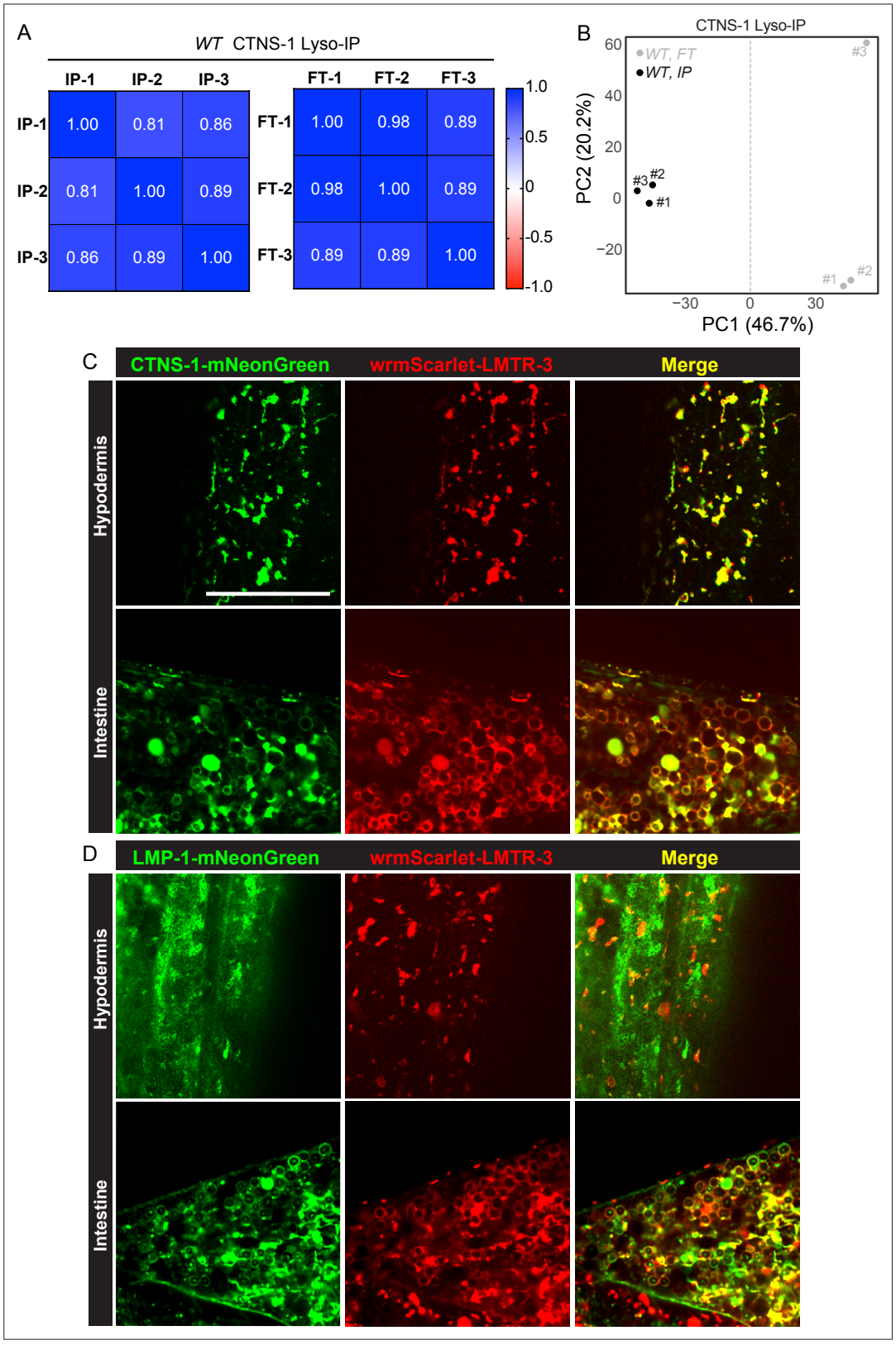

Figure 7—figure supplement 2. CTNS-1 Lyso-IPs and LMTR-3 imaging analyses. (**A**) Correlation analysis of three independent biological replicates of CTNS-1 Lyso-IP (IP) and Flow-through (FT). (**B**) PCA analysis of three independent biological replicates of CTNS-1 Lyso-IP (IP) and Flow-through (FT). (**C, D**) Example images of knock-in lines with wrmScarlet::LMTR-3 and CTNS-1::mNeonGreen (**C**) and LMP-1::mNeonGreen (**D**) in hypodermis and intestine. Scale bar = 20 μm.

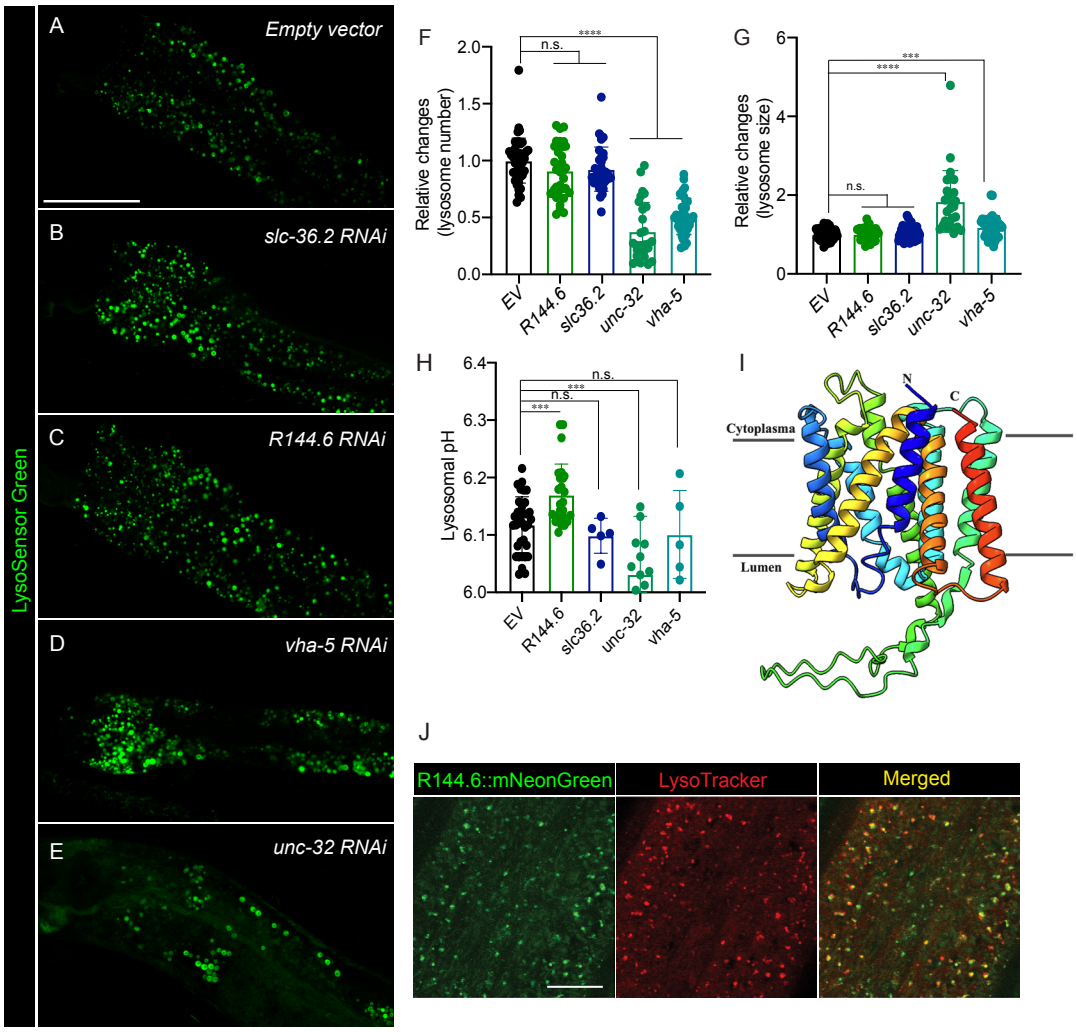

Figure 8. Lysosome-enriched proteins regulating lysosomal functions. (**A-E**) Confocal fluorescence microscopy images of intestinal cells in worms stained with LysoSensor DND-189 and treated with *empty vector* (**A**), *slc36.2* RNAi (**B**), *R144.6* RNAi (**C**), *vha-5* RNAi (**D**) and *unc-32* RNAi (**E**).Scale bar = 50 μm. (**F, G**) RNAi knockdown of *unc-32* or *vha-5* decreases the lysosome number *(****P<0.0001)* (**F**) but increases the lysosome size *(****P<0.0001, *** P<0.001)* (**G**). The average lysosome number and size per pair of intestinal cells were quantified. Data are shown as mean ± standard deviation (SD).

Figure 8 continued on next page

Figure 8 continued

Student *t*-test (unpaired, two-tailed) was performed between the *empty vector* and RNAi-treated groups. At least three independent experiments with ~10 worms in each were performed for each condition. n.s. *P>0.05,* (**H**) RNAi knockdown of *R144.6* and *unc-32 (***P<0.001)* increase and decrease lysosomal pH, respectively. Lysosomal pH was calculated based on LysoSensor's lifetime measured by Fluorescence Lifetime Microscopy. Data are shown as mean ± SD. Student t-test (unpaired, two-tailed) was performed between the *empty vector* and RNAi-treated groups. Two independent experiments with at least 5 worms in each were performed in *R144.6* RNAi and *unc-32* RNAi conditions. The *vha-5* and *slc36.2* RNAi knockdown did not show significant changes in one replicate and were not retested with another replicate. n.s. *P>0.05.*(**I**) The structure of the R144.6 protein predicted by AlphaFold2 supports it as a solute carrier family transporter. (**J**) Confocal fluorescence microscopy images show that mNeonGreen signals from endogenously tagged R144.6 colocalize with LysoTracker Red signals in the hypodermis. Scale bar = 10 μm.

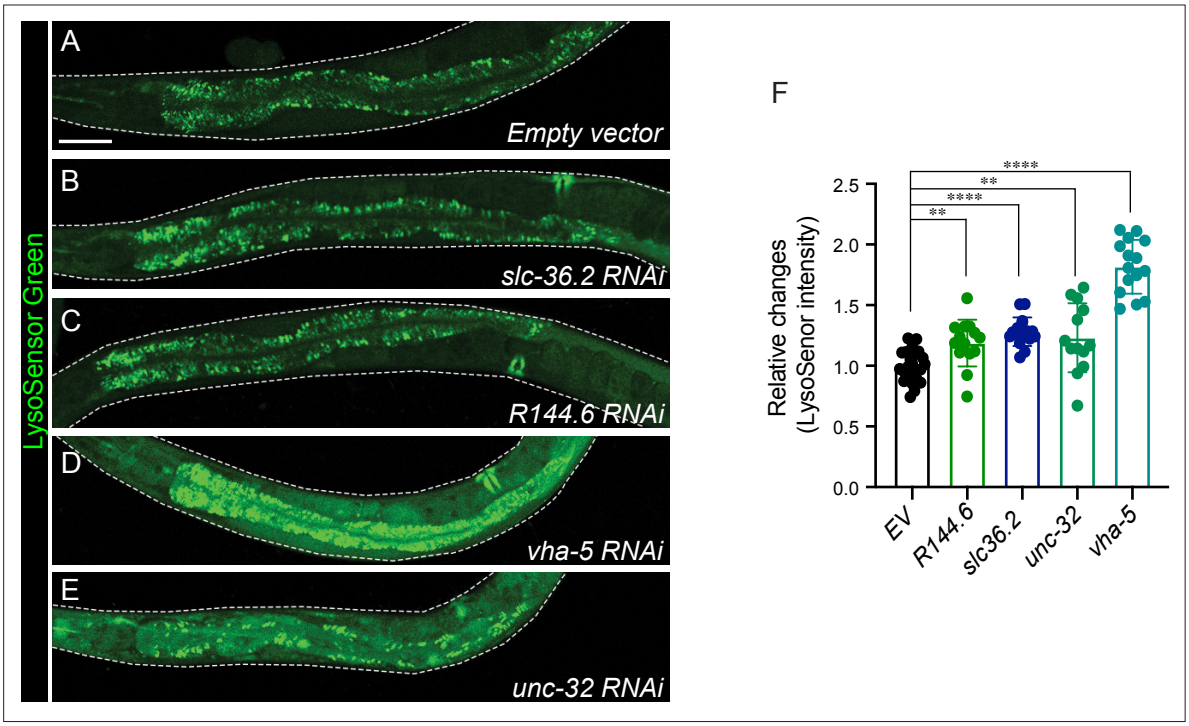

Figure 8—figure supplement 1. LysoSensor intensity quantification in five candidates. The LysoSensor signals are visualized by confocal fluorescence microscopy in *empty vector* (**A**), *slc36.2* RNAi (**B**), *R144.6* RNAi (**C**), *vha-5* RNAi (**D**), and *unc-32* RNAi (**E**) conditions. Scale bar = 50 μm. The relative LysoSensor changes were quantified in (**F**).~10 worms were quantified in each condition. Data are shown as mean ± SD. Student t-test (unpaired, two-tailed) was performed between the *empty vector* and RNAi-treated groups. *(**P<0.01, ****P<0.0001).*